CSMA 2019
14ème Colloque National en Calcul des Structures
13-17 Mai 2019, Presqu'île de Giens (Var)

Impact of the radiation of elastic waves in the soil in a periodic railway track model

H. Pinault[1,2], E. Balmes[2,3], R. Cottereau[4], E. Arlaud[1]

[1] *SNCF Réseau, Direction Générale Industrielle et Ingénierie, 6 Avenue François Mitterrand, 93574 La Plaine Saint Denis Cedex, France. Contact: hadrien.pinault@reseau.sncf.fr*
[2] *Arts et Métiers ParisTech, PIMM, UMR 8006, 151 boulevard de l'Hôpital, 75013 Paris, France*
[3] *SDTools, 44 Rue Vergniaud, 75013 Paris, France*
[4] *Aix-Marseille Univ, CNRS, Centrale Marseille, LMA, UMR 2031, 4 impasse Nikola Tesla, CS 40006, 13453 Marseille Cedex 13*

Abstract — In most railway track models, the soil is modelled as a spring foundation or as a bounded volume (e.g. through the FEM). However, these classical approaches cannot represent with accuracy both the static response and the dynamic behaviour of the track at low frequencies. In this paper, the necessity to include in a track model the radiation of elastic waves in the soil is assessed. It is shown that Perfectly Matched Layers are an efficient solution. Their implementation within a reduced periodic track model and the numerical simulations of a simplified track model are presented.
Keywords — Radiation, Perfectly Matched Layers, railway track, model reduction.

Introduction

Assessing vibration levels in a railway track and its surroundings is a very important industrial issue. Numerical models are an efficient way to study track vibrations. However, the focus is often put on the track itself and the soil is thus modelled as simply as possible: a spring foundation or a bounded volume, through the FEM for instance. Such models are still widely used nowadays [8, 18]. But they elude one fundamental phenomenon: the loss of energy by waves radiated in the soil. The Sommerfeld radiation condition [16] states that the energy radiated from a structure must scatter to infinity and no energy may be radiated from infinity. Neither spring foundation nor finite volume satisfy this fundamental condition, as waves will necessarily reflect at the border of the domain.

The main purpose of this paper is to take the radiation of waves in the track foundation into account. A first approach consists in coupling the FE model of the track superstructure with a Boundary Element (BE) model [11] of the infinite medium. By considering infinite elements, integral equations are solved on the boundary between the periodic medium and the free field thanks to impulse Green functions. This was implemented successfully in many applications [1, 6, 17]. The BEM for elastodynamics being expressed in the frequency domain, this solution has not been chosen in this work.

A common alternative is preferred here: a fictitious absorbing medium, well-known as *Perfecly Matched Layer* (PML) [13], is added to the external boundary of a FEM model of the track. The relaxation of waves passing through the PML is good and small reflexion occurs at the interface or at the new boundary. This FEM/PML coupling has been applied to the railway track by Germonpré and al. [10]. However, this formulation is in the frequency domain, contrary to most dynamic FEM solvers which are time-based, and leads to high computational cost. The time-based formulation proposed in this paper is fully compatible with any dynamic FEM solver and a multi-wavelength model reduction strategy is used.

First of all, in section 1, it is shown with a simple example that classical soil models are insufficient to represent the mechanical behaviour of the track at low frequencies. Then, in section 2, the implementation of the FEM/PML coupling is detailed. In section 3, the reduction strategy of the periodic track model is summarized. Finally the numerical results are discussed in section 4.

1 The necessity to consider the radiation in the soil: a simple example

To emphasize the limitation of track models with spring foundations, a simple model is considered. The superstructure of the track is represented as an Euler-Bernoulli infinite beam in x direction, lying on an elastic foundation of stiffness k_S, and excited in bending with a localized force Q at the point $x = 0$, in the $-z$ direction. The equation of motion for displacement $u(x,t)$ is

$$\rho S \frac{\partial^2 u}{\partial t^2}(x,t) + EI \frac{\partial^4 u}{\partial x^4}(x,t) + k_s u(x,t) = -Q\delta(x),$$

where E is the Young's modulus of the beam, I its moment of inertia, ρ its density and S its cross-section. Then the ratio of displacement over applied force at point $x = 0$, known as *receptance*, has the following analytical expression

$$|H(\omega)| = \frac{1}{2\sqrt{2}(EI)^{1/4}|\rho S\omega^2 - k_S|^{3/4}}.$$

This receptance is plotted in figure 1a with $\rho S = 106$ kg/m, $EI = 22.4$ kPa·m^2 and $k_S = 5$ MN/m. To represent with accuracy the low frequency response of the track, two fundamental quantities have to be computed: the static response of the track and the resonance of the track on its foundation. First the static response has the analytical expression $|H(0)| = \frac{1}{2\sqrt{2}(EI)^{1/4}k_S^{3/4}}$. The only free parameter k_S can be tuned to represent the experimental static response (dotted red line in figure 1a). Then, the resonance of the track (dashed green line in figure 1a) is equal to $\sqrt{\frac{k_S}{\rho S}}$ and cannot be fitted on experimental results. The introduction of a damper does not modify the static response, and the resonance peak is just slighty modified: to move the peak to a far value, the associated damping will be excessively high. Also, volumic models have the same fundamental issue, as the portion of soil acts at low frequencies like an equivalent spring whose stiffness only depends on the size of the model (mechanical parameters of the soil being already fixed by the experimental values).

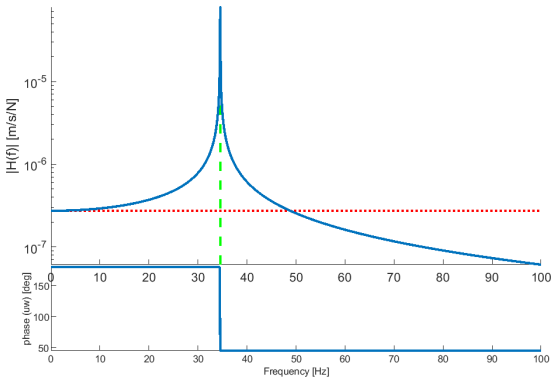

(a) Receptance of a beam on an elastic foundation. The red dotted line correspond to the static response, and the green dashed line to the resonant frequency.

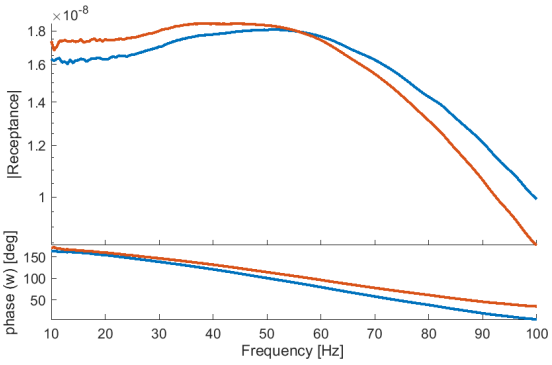

(b) Experimental receptances obtained on a ballasted track on the Chauconin site for 2 tests.

Figure 1: Experimental and analytical receptances of a railway track.

To have an idea of expected results, two experimental curves from Arlaud et al. [2] are presented in figure 1b. The experiments were performed on a High Speed Line at the Chauconin site. The first resonance of the superstructure on the soil is visible around 40-50 Hz but seems very much damped. Compared to the simple model in figure 1a, it is clear that fitting the model on this experimental values will lead to non-physical damping values. In fact, the *radiation* of waves (and the related loss of energy at infinity) is mainly responsible for what seems to be damping. The constant decrease of the phase is also a characteristic of the low frequency behaviour of the track.

This simple example highlights the lack of information when omitting the radiation of waves at infinity, and the necessity to take this phenomenon into account, e.g. by PML or BEM.

2 Time-based FEM/PML coupling implementation

In this paper, a periodic model of the track is considered, i.e. the global domain Ω is composed of $N+1$ disjoint cells Ω_n obtained from a reference cell Ω_0 only by a translation along the x-axis: $\Omega = \bigcup_{n\in[0\ N]} \Omega_n$. In this section, the coupling of FEM and PML is considered only in the reference cell Ω_0. The extension to the global system Ω is dealt in the following section 3.

2.1 Reference cell for the periodic track model

As shown on figure 2a, both the superstructure (rail, sleeper, ballast) and the foundation (form layer and natural soil) are included in the reference cell Ω_0. The soil size is arbitrary whereas the thickness of the track in the periodic direction is $L_x = 0.6$m as the usual sleeper spacing. Each element of the track is supposed visco-elastic and isotropic, with the mechanical properties described in table 1.

Table 1: Table of material properties.

		Young Modulus	Poisson Ratio	Density	Loss factor
1	**Rail**	210 GPa	0.3	7800 kg/m^3	0
2	**Sleeper**	30 GPa	0.25	2400 kg/m^3	0
3	**Ballast**	250 MPa	0.2	1700 kg/m^3	0.07
4	**Form layer**	544 MPa	0.35	2000 kg/m^3	0.01
5	**Soil**	67 MPa	0.3	1800 kg/m^3	0.01

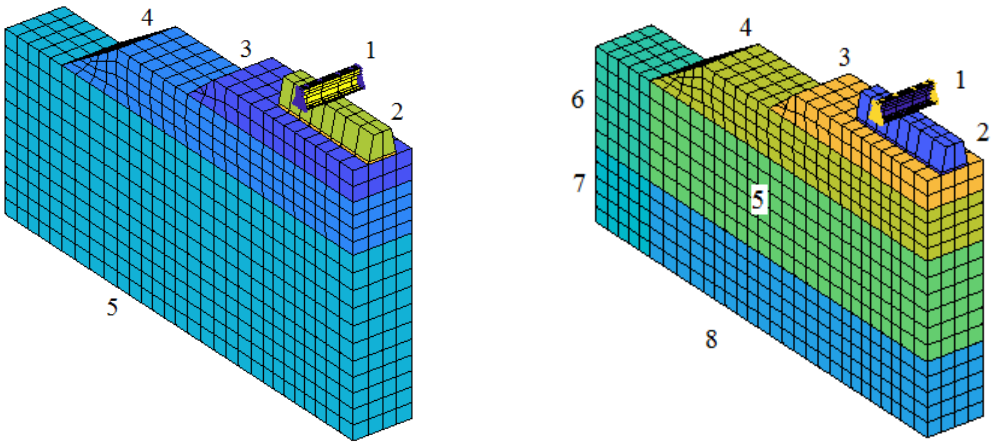

(a) Materials of the model. Each label corresponds to the material properties in table 1.

(b) Properties of the model. Each label corresponds to a different medium.

Figure 2: Half reference cell for the periodic track model with PML.

In the following, the Degrees Of Freedom (DOF) of Ω_0 are split into 3 disjoint groups: the interior of the classical medium (labelled 1-5 in figure 2b), the PML (labelled 6-8) and the interface. They will be denoted respectively m, p and i.

2.2 Equations of motion in the classical material

In this subsection, the union of the classical material m and the interface i is considered. It is assumed that no force is applied at the interface. With the elasticity hypothesis, the elastic tensor $\mathbf{D}$ for each material of the track depends only on the Young modulus E and Poisson ratio ν. With a small loss factor $\eta \ll 1$, the visco-elastic behaviour is approximated by a complex Young modulus $E^* = E(1+i\eta)$. The

equations of motion are then

$$\begin{cases} \rho\ddot{\mathbf{u}}(\mathbf{x},t) = \boldsymbol{\nabla}\cdot\boldsymbol{\sigma}(\mathbf{x},t) + \mathbf{f}(\mathbf{x},t) \\ \boldsymbol{\sigma} = \mathbf{D} : \varepsilon \\ \varepsilon[\mathbf{u}] = \frac{1}{2}\left(\boldsymbol{\nabla}\mathbf{u} + \boldsymbol{\nabla}\mathbf{u}^T\right), \end{cases}$$

where $\mathbf{f}$ are the volumic forces.

After a Finite Element (FE) discretization, the equations of motion in the classical material can be written in a matrix system such as

$$\begin{bmatrix} m_{mm} & m_{mi} \\ m_{mi}^T & m_{ii} \end{bmatrix} \begin{Bmatrix} \ddot{q}_m \\ \ddot{q}_i \end{Bmatrix} + \begin{bmatrix} k_{mm} & k_{mi} \\ k_{mi}^T & k_{ii} \end{bmatrix} \begin{Bmatrix} q_m \\ q_i \end{Bmatrix} = [b] \begin{Bmatrix} F(t) \\ 0 \end{Bmatrix}, \tag{1}$$

where $\{q\}$ are the nodal displacement, $[b]$ the spatial component of the applied loads (volumic and at the boundaries) and $\{F\}$ their time component.

2.3 Equations of the PML

Now the equations of motion in the PML are considered. As they have exactly the same mechanical properties as the classical material, no reflection theoretically occurs at the interface and waves are exponentially damped to a negligible value. Of course, the size and the parameters of the discretized PML are very important to fulfill as much as possible these properties. In this paper, the time-based formulation of Festa and Vilotte [9] is chosen because it is compatible with the time-based solvers. The frequency-domain approach exists [5].

In each direction x_k of space, a relaxation function has to be defined. In this paper, a simple quadratic polynomial is chosen:

$$\alpha_k(x_k) = \alpha_k^0 \left(\frac{x_k - x_k^0}{L_k^P}\right)^2, \forall x_k > x_k^0, \tag{2}$$

where x_k^0 is the coordinate of the interface, L_k^P the total length of the PML in x_k-direction and α_k^0 the relaxation frequency. The relaxation is null in tangential directions to the interface. In the time-based formulation of the PML, convolution products naturally appear but are very costly in terms of computation time and memory. To avoid this issue, Festa and Vilotte [9] proposed a dual formulation in stress/displacement with split variables in the three directions of space:

$$\mathbf{u}(\mathbf{x},t) = \sum_{k=1}^{3} \mathbf{u}^k(\mathbf{x},t), \qquad \boldsymbol{\sigma}(\mathbf{x},t) = \sum_{k=1}^{3} \boldsymbol{\sigma}^k(\mathbf{x},t). \tag{3}$$

With variables from equation (3), the equations of motions can be written as

$$\rho\left(\ddot{u}_i^k(\mathbf{x},t) + \alpha_k(x_k)\dot{u}_i^k(\mathbf{x},t)\right) = \frac{\partial \sigma_{ik}}{\partial x_k}(\mathbf{x},t), \tag{4a}$$

$$\dot{\sigma}_{ij}^k(\mathbf{x},t) + \alpha_k(x_k)\sigma_{ij}^k(\mathbf{x},t) = \sum_{l=1}^{3} D_{ijkl}\frac{\partial \dot{u}_l}{\partial x_k}(\mathbf{x},t). \tag{4b}$$

With the symmetry properties of the elastic tensor, the three coordinates $\sigma_{23}^1, \sigma_{13}^2$ and σ_{12}^3 are always null. There are still $(3+5)\times 3 = 24$ unknown fields, which explains the higher computational cost and memory required for a PML element in comparison to a classical element with 3 unknown fields.

A Ritz-Galerkin discretization is applied to equations (4). The displacement $\{u\}$ (resp. the strain tensor $\{\sigma\}$) is computed from nodal displacements $\{q\}$ thanks to form functions $[N]$ (resp. $[B]$)

$$\{u(\mathbf{x},t)\} = [N(\mathbf{x})]\{q(t)\}$$

$$\{\varepsilon(\mathbf{x},t)\} = \begin{Bmatrix} \varepsilon_{11} & \varepsilon_{22} & \varepsilon_{33} & \varepsilon_{23} & \varepsilon_{13} & \varepsilon_{12} \end{Bmatrix}^T = [B(\mathbf{x})]\{q(t)\}\ .$$

To get a more convenient formulation, the variable $\mathbf{s}^k$ such as $\boldsymbol{\sigma}^k = \dot{\mathbf{s}}^k$ is preferred. All calculations done, the matrix system can be written as

$$\begin{bmatrix} M_q & 0 & 0 & 0 & 0 & 0 \\ 0 & M_q & 0 & 0 & 0 & 0 \\ 0 & 0 & M_q & 0 & 0 & 0 \\ 0 & 0 & 0 & M_s & 0 & 0 \\ 0 & 0 & 0 & 0 & M_s & 0 \\ 0 & 0 & 0 & 0 & 0 & M_s \end{bmatrix} \begin{Bmatrix} \ddot{q}_p^1 \\ \ddot{q}_p^2 \\ \ddot{q}_p^3 \\ \dot{s}_p^1 \\ \dot{s}_p^2 \\ \dot{s}_p^3 \end{Bmatrix} + \begin{bmatrix} C_{q1} & 0 & 0 & b_{s1} & b_{s1} & b_{s1} \\ 0 & C_{q2} & 0 & b_{s2} & b_{s2} & b_{s2} \\ 0 & 0 & C_{q3} & b_{s3} & b_{s3} & b_{s3} \\ b_{s1}^T & b_{s1}^T & b_{s1}^T & C_{s1} & 0 & 0 \\ b_{s2}^T & b_{s2}^T & b_{s2}^T & 0 & C_{s2} & 0 \\ b_{s3}^T & b_{s3}^T & b_{s3}^T & 0 & 0 & C_{s3} \end{bmatrix} \begin{Bmatrix} \dot{q}_p^1 \\ \dot{q}_p^2 \\ \dot{q}_p^3 \\ s_p^1 \\ s_p^2 \\ s_p^3 \end{Bmatrix} = \{0\}. \quad (5)$$

The matrices used in equation (5) are defined by

$$[M_q] = [N_q]^T [\rho] [N_q], \qquad [M_s] = [N_s]^T [D]^{-1} [N_s], \qquad \left[C_{qk}\right] = [N_q]^T [\rho\alpha_k] [N_q],$$
$$[C_{sk}] = [N_s]^T \left[D^{-1}\alpha_k\right] [N_s], \qquad [b_{sk}] = [B_k]^T [N_s],$$

for $k = 1,2,3$, where $[B_k]$ are obtained from $[B]$ by preserving only the derivatives along the x_k-direction. Notice that the stress-related variables $\left\{s^k\right\}$ are evaluated at the nodes, and not at Gauss points as in classical FEM formulation.

2.4 Coupling FEM and PML

For now on, the equations (1) and (5) seem to be fully decoupled. Indeed, the continuity relation of the nodal displacements at the interface needs to be considered. Its expression is

$$\{q_i\} = \sum_{k=1}^{3} \left[c_i^k\right] \left\{q_p^k\right\}, \quad (6)$$

where the $\left[c_i^k\right]$ are appropriate observation matrices. The global system matrix is obtained by eliminating $\{q_i\}$ from equation (1) thanks to (6), and combining the resulting system with (5). No continuity relation is necessary on variables $\{s_p\}$ as the relaxation function is always null on the interface.

3 Periodic, reduced track model with absorbing boundaries

From now, the whole periodic structure Ω is considered. Because the size of the resulting system is huge, it is interesting to do model reduction. To find a reduction basis that complies with the periodicity of the model, it is useful to split the equations of motion obtained in section 2 along internal DOFs and left/right interface DOFs. They will be noted respectively I, L and R. Also, because the model reduction process is based on modal analysis, it is necessary to switch temporarily to the frequency domain. Thus the dynamic stiffness matrix $[Z] = -\omega^2 [M] + i\omega [C] + [K]$ is considered.

Such a periodic structure is often assimilated as a *waveguide* and wave-related methods like the Wafe Finite Element (WFE) method [14] are used. In this method, a frequency ω_0 is fixed and the wavenumbers $\kappa_j(\omega_0)$ corresponding to propagative and weakly evanescent waves are searched. In this paper, an alternative is chosen, taken from the work of Arlaud [3]: a wavenumber κ_0 is fixed and modes at frequencies $\omega_j(\kappa_0)$ are searched. This choice allows a clear truncature of the modes (taken from classical modal analysis) necessary to perform model reduction, whereas the selection of waves in the WFE method is rather uncertain. It is not the purpose of this paper to fully describe this reduction procedure, however the main steps are given for a better understanding.

1. *Subspace learning phase*: a few wave-numbers κ_j are selected (typically a high value around 1 cell^{-1} and a low value around $\frac{1}{50}$ cell^{-1}). For each wave-number κ_j, modes $\left\{\phi_k(\kappa_j)\right\}$ are computed from the equation

$$[T_c(\kappa_j)]^T [Z(\omega_k)] [T_c(\kappa_j)] \left\{\phi_k(\kappa_j)\right\} = \{0\},$$

where $[T_c]$ is a basis used to verify the continuity relation $\left\{q_L^{n+1}\right\} = \left\{q_R^n\right\}, \forall n \in [0\ N]$. Only the eigenvalues $\omega_k(\kappa_j)$ below a limit $\omega_{\max}$ are selected to obtain a reduced basis $[\Theta]$. Also, a static correction is included in $[\Theta]$ to take into account the residual flexibility of high frequency modes.

2. *Basis formatting*: the basis $[\Theta]$ has no chance to be compatible with the specific geometry of the periodic cell model. To comply with the geometry, $[\Theta]$ is first split along the DOF into $\begin{bmatrix}\Theta_L & \Theta_I & \Theta_R\end{bmatrix}$. Then the desired basis $[T_L]$ and $[T_R]$ is obtained from a Singular Value Decomposition (SVD) of span(Θ_L, Θ_R). Only most significant singular values are selected. Finally the Schur complement method [12] is applied to finish the basis construction with $[T_I]$.

From the reduced basis $[T]$, generalized coordinates can be defined with $\{p\} = [T]^T \{q\}$. The reduced system is obtained after going back to the time domain and multiplying by $[T]^T$:

$$\left([T]^T [M] [T]\right) \{\ddot{p}\} + \left([T]^T [C] [T]\right) \{\dot{p}\} + \left([T]^T [K] [T]\right) \{p\} = [T]^T \{F\}. \tag{7}$$

Assuming that the responses of the track are within the considered subspace, the reduction must be done only once.

4 The dynamic behaviour of a railway track at low frequencies

To assess the validity of the implementation developed in this paper, the computation of the receptance of the track is done with a full FEM model, and a coupled FEM/PML model. As a preliminary result, only a very coarse model of the track is used. The purpose of this work is simply to highlight the influence of the PML within a track model, and not to give predictive results.

The simple track model shown in figure 2 is studied in two configurations : with a deep soil of 10m and no PML (configuration A); and with a soil of 3m and PML (configuration B). In the model B, the relaxation frequency (see equation (2)) has been fixed to

$$\alpha_k^0 \simeq \frac{10 c_p}{L_k^P} = \frac{10}{L_k^P} \sqrt{\frac{E(1-\nu)}{\rho(1+\nu)(1-2\nu)}},$$

following the work of Collino et Tsogka [7]. They proved that this value leads to an optimum of the efficiency of the PML. The choice of the PML length is still an open question, and thus has been fixed arbitrarily to 17m. Both configurations have clamped boundaries, except for the faces orthogonal to the axis of the track where periodicity relations are applied. A vertical excitation is applied uniformly on the top surface of the track and the response is computed in space and time.

In figure 3, the results for both models are presented in two complementary ways :

- The amplitude of the Fourier transform in space and time (2D-FFT) of the response. The wave-number is scaled by the length of the cell 0.6m and thus expressed in cell^{-1}. A logarithmic map is chosen, with bright yellow colors for the maximum of amplitude, and dark blue for the minimum.
- The receptance of the track, which is computed as the integral of the 2D-FFT on the wave-numbers. It is placed just above the 2D-FFT to ease the comparaison.

Without PML, a first peak in the receptance (figure 3a) appears around 10 Hz and corresponds to the main curve in the 2D-FFT (figure 3c). The peak is quite narrow, which is related to the slow evolution of the 2D-FFT curve. It can be interpreted as the first mode of the superstructure on the soil. Other peaks are present at higher frequencies, which correspond to the other curves on the 2D-FFT: these are the modes of higher order, that do not exist in an infinite soil.

To the contrary, with PML, only one curve is present in the 2D-FFT (figure 3d): unwanted soil modes are no longer present. Moreover this curve is quite linear and has a important evolution on frequencies: it can be linked to the radiation of a wave in the soil. For now, only a coarse computation has been tested and more precise computations are in progress. This unique curve results in a very broad peak in the corresponding receptance curve (figure 3b). This is solely the consequence of the radiation modeled by PMLs, and should not be linked with damping.

Comparing this preliminary results with the expectations of experimental data (see figure 1b), the authors are confident that this FEM/PML coupling will lead to more accurate results in the computational analysis of the railway track.

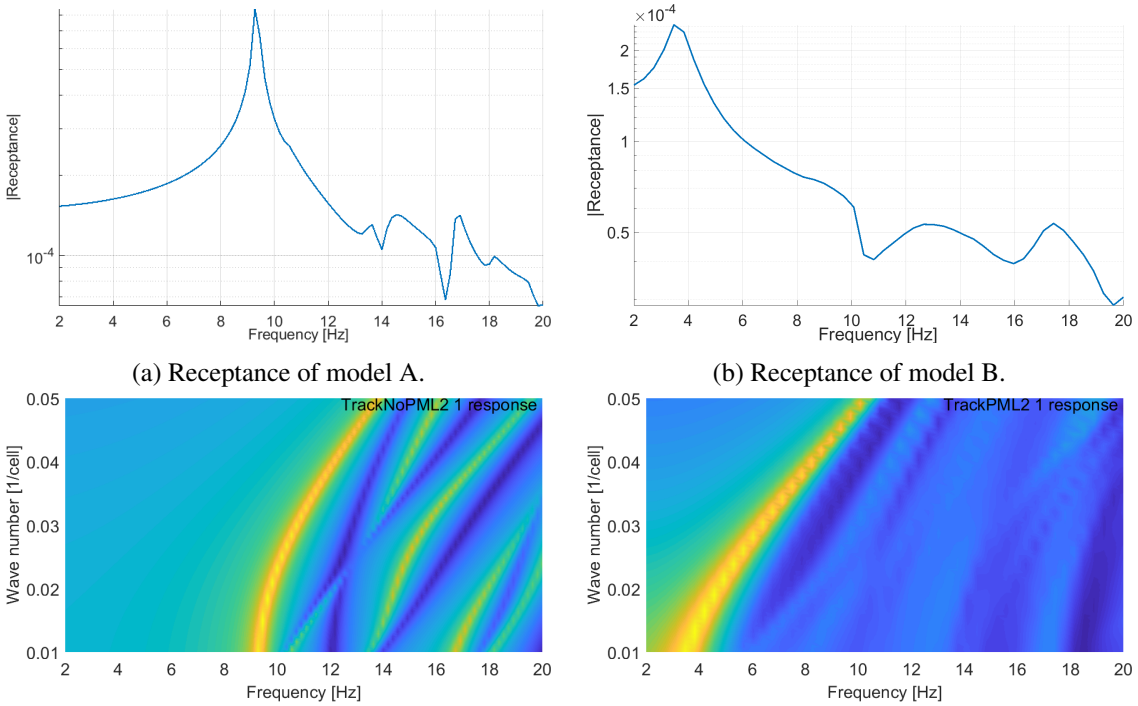

(a) Receptance of model A.

(b) Receptance of model B.

(c) 2D-FFT of model A.

(d) 2D-FFT of model B.

Figure 3: 2D Fourier transform of a simplified track model with (A) and without PML (B).

Conclusion

In this paper, it has been shown that the radiation of elastic waves in the soil is an important phenomenon that cannot be neglected in track models. A time-based implementation of the FEM/PML coupling has been detailed, within a periodic track model. This formulation is compatible with any FE solver and allows an easier and efficient model reduction, based on modal analysis. This methodology can be applied to any periodic structure lying or inserted in an infinite medium: e.g. a road, a tunnel or a buried pipe.

References

[1] P. Alves Costa, R. Calçada and A. Silva Cardoso, *Track-ground vibration induced by railway traffic: In-situ measurements and validation of a 2.5D FEM-BEM model*, Soil Dynamics and Earthquake Engineering 32 (1), pp. 111-128, 2012.

[2] E. Arlaud, S. Costa d'Aguiar and E. Balmes, *Receptance of railway tracks at low frequency: Numerical and experimental approaches*, Transportation Geotechnics 9, pp. 1-16, 2016.

[3] E. Arlaud, *Modèles dynamiques réduits de milieux périodiques par morceaux : application aux voies ferroviaires*, PhD Thesis (in French), Ecole Nationale Supérieure d'Arts et Métiers, 2016.

[4] E. Balmes, *Model reduction for systems with frequency dependent damping properties*, in IMAC, 1997.

[5] U. Basu and A.K. Chopra, *Perfectly matched layers for time-harmonic elastodynamics of unbounded domains: theory and finite-element implementation*, Computer Methods in Applied Mechanics and Engineering 192, pp. 1337-1375, 2003.

[6] D. Clouteau, M. Arnst, T.M. Al-Hussaini and G. Degrande, *Freefield vibrations due to dynamic loading on a tunnel embedded in a stratified medium*, Journal of Sound and Vibration 283, pp. 173-199, 2005.

[7] F. Collino and C. Tsogka, *Application of the perfectly matched absorbing layer model to the linear elastodynamic problem in anisotropic heterogeneous media*, Geophysics 66 (1), pp. 294-307, 2001.

[8] Z. Dimitrovová, *Critical velocity of a uniformly moving load on a beam supported by a finite depth foundation*, Journal of Sound and Vibration 336, pp. 325-342, 2016.

[9] G. Festa and J.-P. Vilotte, *The Newmark scheme as velocity-stress time-staggering: an efficient PML implementation for spectral element simulations of elastodynamics*, Geophysical Journal International 161 (3), pp. 789-812, 2005.

[10] M. Germonpré, G. Degrande and G. Lombaert, *Periodic track model for the prediction of railway induced vibration due to parametric excitation*, Transportation Geotechnics 17, pp. 98-108, 2018.

[11] W.S. Hall, *The Boundary Element Method*, Springer Netherlands, 1994.

[12] *Harris' Shock and Vibration Handbook*, A.G. Piersol and T. L. Paez editors, 6th Edition, McGraw-Hill Handbooks, 2009.

[13] D. Komatitsch and J. Tromp, *A perfectly matched layer absorbing boundary condition for the second-order seismic wave equation*, Geophysical Journal International 154 (1), pp. 146-153, 2003.

[14] J.-M. Mencik and D. Duhamel, *A wave-base model reduction technique for the description of the dynamic behavior of periodic structures involving arbitrary-shaped substructures and large-sized finite element models*, Finite-Element in Analysis and Design 101, pp. 1-14, 2015.

[15] A. Modave, E. Delhez and C. Geuzaine, *Optimizing perfectly matched layers in discrete contexts*, International Journal for Numerical Methods in Engineering 99, pp. 410-437, 2014.

[16] S.H. Schot, *Eighty years of Sommerfeld's radiation condition*, Historia Mathematica 19, pp. 385-401, 1992.

[17] V.V. Yotov, M. Remedia, G.S. Aglietti and G. Richardson, *Efficient matrix randomisation methodology for reduced spacecraft models in stochastic FEM-BEM vibroacoustic problems*, in European Conference on Spacecraft Structures, Materials and Environmental Testing, 2018.

[18] Q. Xu, Z. Xiao, T. Liu, P. Lou and X. Song, *Comparison of 2D and 3D prediction models for environmental vibration induced by underground railway with two types of tracks*, Computers and Geotechnics 68, pp. 169-183, 2015.